e-ISSN: 2146 - 9067

International Journal of Automotive Engineering and Technologies

journal homepage:
https://dergipark.org.tr/en/pub/ijaet

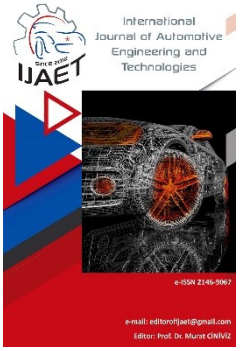

Original Research Article

Analysis and optimization of interior permanent magnet synchronous motor for electric vehicle applications using ANSYS Motor-CAD

Doğukan Ayhan[1, *]

[1, *] Manisa Celal Bayar University, Engineering Faculty Department of Electrical and Electronics Engineering, Manisa, Türkiye.

ARTICLE INFO

Orcid Numbers
1. 0000-0002-7111-7260

Doi: 10.18245/ijaet. 1247462

* Corresponding author

doguzeus@gmail.com

Received: Feb 03, 2023
Accepted: Sep 18, 2023

Published: 30 Sep 2023

Published by Editorial Board Members of IJAET

ABSTRACT

The Permanent Magnet Synchronous Motor (PMSM) has the capability to high torque to current ratio, high power to weight ratio, high efficiency and stability. Due to the above positive points, PMSM is extensively employed in recent variable speed AC drives, particularly in electric vehicle applications. The electric vehicle is convenient for the city traffic without toxic gas emissions with low noise. PMSM became at the top of AC motor types due to the positive features written in the previous lines. However, it has two major drawbacks i.e. high cost and small speed range but it can be controlled and exceed to the small speed range with some control methods. A radial flux inner rotor PMSM architecture for electric vehicle application is presented in the project. The Interior Permanent Magnet Synchronous Motor (IPMSM) of the electric vehicle Leaf model, which was first produced by Nissan company in 2012, will be analyzed with ANSYS Motor-CAD and then the analysis results will be compared with the theoretical results and finally will be optimized in the project. The paper will provide insights about various change of parameters and their effects to the other parameters.

Keywords: Analysis, Optimization, Finite Element Analysis, Electric Vehicle, Radial flux, ANSYS Motor-CAD, Permanent Magnet Synchronous Motor, Interior Permanent Synchronous Motor

1. Introduction

(PMSM) finds uses in numerous industries such as traction applications or when high dynamic performance is required, electric vehicles, robotics and aerospace technologies. The power density of PMSM is higher than induction motor with the fewer core losses due to placed permanent magnets in rotor section and the PMSM can generate torque due to permanent magnets at zero speed moment. Nowadays, permanent magnet synchronous motor is built not only to be more powerful but also with reduced mass and lower moment of inertia. PMSM is a sort of synchronous motor that high magnet material is used to magnetize to rotor part of machine, it has some features such as high efficiency, simple structure, easy to regulate and so on. Inverter fed PMSM drive systems have made it come true to eliminate the physical contact between the mechanical brushes and commutators, so it has become a

feasible choice for motion control applications such as robotics, electric vehicle application, electricity generation, aerospace, and etc. Inverter fed PMSM have been widely used in industry with the quick development of power electronic and lowering price of electrical parts. The PMSM is directly fed by the inverter, phase windings are connected to the output of the inverter and PMSM's input voltage is manipulated through the inverter. There are 3 zones when we look at the PMSM torque-speed graph: constant torque, constant power and power decreasing. The transition from the first zone, the constant torque zone, to the second zone, the constant power zone, takes place after the rated speed is exceeded. Here, using the Flux Weakning technique, a transition is made over the rated speed zone. Once this transition is achieved, optimum current, flux, torque and speed values are determined using the motor driver and also PMSM has sinusoidal back EMF while BLDC motor has trapezoidal back EMF [1, 2]. Another issue, electromagnetic steel sheet of stator and rotor core less than 0.35 mm in thickness is generally used for the stator core because of the need to reduce iron loss during high-speed motor operation in electrical vehicles. The typical method of assembling the cores of stator and rotor involve caulking and stacking sheets(lamination) that have been continuously created through high-speed stamping. A sheet thickness of 0.2 mm causes issues with economy and productivity in the caulking process because the sheets are excessively thin but a sheet thickness of 0.35 mm causes a problem with excessive heat generation at high motor speeds compare to 0.2 and 0.3. In this project, a sheet thickness of 0.3 mm was chosen for the stator to prevent these problems since it has a lower iron loss than a thickness of 0.35 mm and makes caulking easier. The stacking factor was calculated for both of cores. PMSM is inevitable especially in areas that produce low speed and high torque or are required. For example, various PMSM's can be designed for electricity generation in river regions, including wind turbines. That's why, the machine gives a constant torque in the constant torque region, that is under the nominal speed shown in Figure-1. On the other hand, this motor type is inevitable in electric vehicle applications because of the advantages mentioned in the previous lines and the energy consumption of PMSM is very low, so it is used in green vehicles. The awareness of green and electric vehicle improves the PMSM [3]. In this analysis, interior permanent magnet synchronous motor (IPMSM) was analyzed that can be used for electric vehicles in depth because IPMSM is appealing for applications requiring a wide speed range [4]. Unlike surface mounted permanent magnet motor (SMPMSM), which have the same inductance in the d and q axes. Therefore, this causes all the torque to be generated by the magnetic flux. Interior permanent magnet motors have varying d and q inductances, resulting in an extra torque component known as reluctance torque. The best parameters were tried to find with optimization technique in this paper.

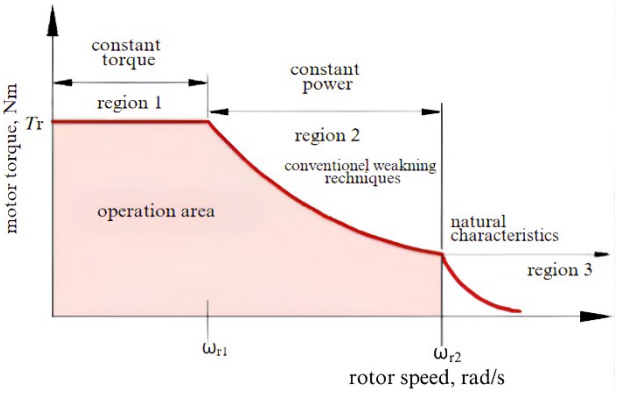

Figure 1: The operation characteristic of PMSM [2]

2. Construction and Types of PMSM

PMSM is brushless and the efficiency and reliability are very high for this sort of AC synchronous motor. The field excitation of PMSM is provided by the permanent magnets in rotor part and stator part is fed by the inverter with 3 phase outputs. The main difference between PMSM and induction motor is in rotor part and is due to permanent magnets. PMSM is a hybrid between an induction motor and a brushless DC motor. Also, the stator structure with windings made to produce a sinusoidal flux density in the air gap of the machine is similar to the stator of an induction motor [1]. PMSM is structurally a synchronous motor and there are permanent magnets in the rotor part. The placement of permanent magnets in the rotor part can be examined under two classes as SMPMSM and IPMSM. In the paper, the IPMSM was preferred because it has higher durability and stability at high speeds compared

to the SMPMSM type, when the PMSM reaches high speeds, a centrifugal force will form inside the PMSM and this type of rotor is generally preferred to protect to the PMSM from this centrifugal force [1]. As a result, decided to design, analyze and optimize an IPMSM with double layer magnets and a distributed winding. The motor design in the project produces 10 percent greater torque than the conventional single-layer magnet IPMSM operating on the same current and the same kind of winding because of more magnetic flux in rotor and this effect to permanent magnet torque in motor. The various views of pattern shown in Figure-2 a, b.

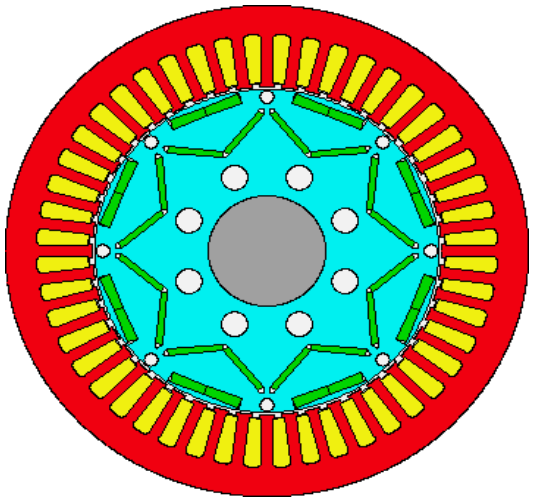

Figure 2: a) IPMSM 2D-radial front view

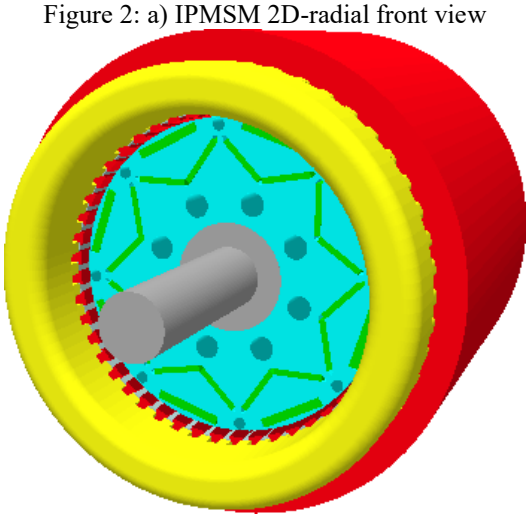

Figure 2: b) IPMSM 3D-view

3. Working Principle of IPMSM

The permanent magnets provide lossless excitation without any external electrical circuit. They are often used in DC excitation circuits in synchronous generators to provide field excitation. A rotating magnetic field is produced by the three-phase symmetrical AC fed windings of the stator in the air gap. The rotor's field must follow the stator's field and rotate at the same synchronous speed to produce a constant average torque. Three phase windings similar to that of the induction motor are supplied with sinusoidal currents for the PMSM model when the motor is started. The currents create a magnetic field that rotates at the same or synchronous speed as the rotor. The speed of the rotor can be adjusted accordingly by adjusting the frequency of the stator current. The stationary magnetic field of the permanent magnet of the field excitation changes rotationally and as a result of this change an EMF is induced in the opposite direction. This is called Back EMF in the literature. This can explain with Ampere's Law as given with equation (1) [5].

$$\nabla x\mathbf{H} = \mathbf{J} + \frac{\mathbf{dD}}{\mathrm{dt}} \quad (1)$$

4. Construction Details

4.1. Airgap flux density

The definition focuses more on permanent magnet rotor design. Also, a slotted stator is used in the design, so this is assumed. The air gap flux density (B) is limited by the saturation of the stator core. In particular, the maximum flux density is limited by the width of the teeth, while the stator back determines the total maximum flux. Also, the saturation level allowed depends on the application limits. Generally, the flux density is lower on high efficiency machines and higher on machines designed for maximum torque density. The magnetic flux density(B) value is high for ferromagnetic materials. The peak air gap B is typically in the range of from 0.7 T to 1.1 T [3]. It should be noted that this is the total B, i.e the sum of the rotor and stator flux densities. The airgap is between the rotor outer diameter and the stator inner diameter. Therefore, the rotor and stator magnetic flux lines pass through the air gap. The reaction is smaller, which means higher reluctance torque. However, in order to obtain a large reluctance torque contribution, the stator reaction must be large. There are mainly two torques, reluctance torque and magnet torque in IPMSM. It is very important to obtain a good alignment or reluctance torque. Reluctance torque is the result of the interaction of the rotor and the stator of the motor. Inductance (L) values should be low for good

reluctance torque. Airgap distance selection is very important because this parameter affects various output parameters of the motor. The optimization for the airgap distance was carried out in the optimization section of the paper.

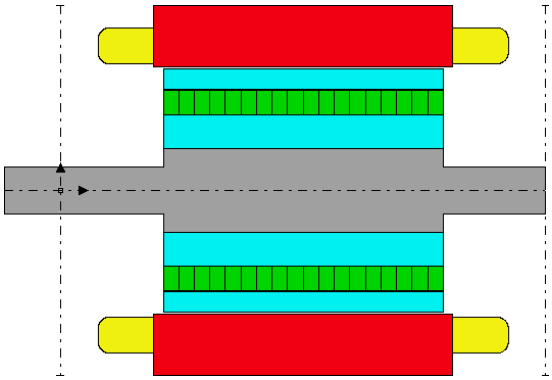

Figure 2.2: IPMSM 2D-axial view

4.2. Permanent magnet materials for design IPMSM

Currently, attention is focused on materials based on rare earth metals and transition metals. These materials allow obtaining permanent magnets with high magnetic properties. Depending on the technology, magnets are characterized by different magnetic and mechanical properties and show different corrosion resistance. Strong magnets have a low magnetic flux density value and a large magnetic flux value. That's why, that is difficult to magnetize and demagnetize materials with strong magnetism. The strongly magnetized materials maintain their magnetic properties up to the Curie temperature and the maximum threshold current value to be exposed [1]. Neodymium Iron Boron (NdFeB) and Samarium Cobalt (SmCo) magnets are the most advanced commercial permanent magnet materials available on today. Neodymium Iron Boron magnets were introduced commercially in the early 1980s [6]. They are widely used today in many different applications. The cost of this magnet material is comparable to ferrite magnets. neodymium magnets cost about 10 to 20 times more. Some important features used to compare ferrite magnets with permanent magnets are; residue (Mr) which measures the strength of the magnetic field coercivity (Hci), resistance of the material to demagnetization energy product (BHmax), density of magnetic energy and Curie temperature (TC). The temperature at which the material loses its magnetism and etc. Neodymium magnets have higher persistence, much higher coercivity and energy product but generally have a lower Curie temperature than other materials. Neodymium is alloyed with terbium and dysprosium to maintain its magnetic properties at high temperatures [3].

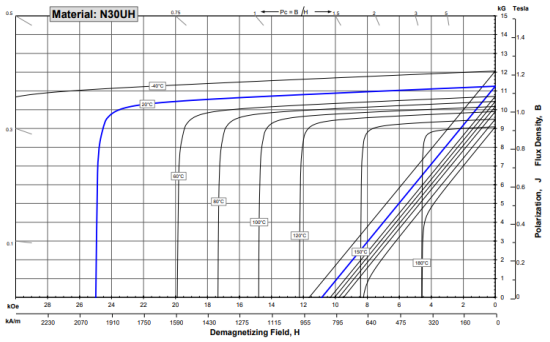

Figure 3: B-H curves of N30UH material under various temperatures

Table-1: a) Magnetic characteristics of N30UH [7]

Magnetic Characteristics	Units	Min.	Nominal	Max.
Br, Residual Induction	Gauss	10.800	11.250	11.700
	mT	1080	1125	1170
H_{cB}, Coercivity	Oersteds	10.200	10.700	11.200
	kA/m	812	852	891
H_{cJ}, Intrinsic Coercivity	Oersteds	25.000	-	-
	kA/m	1.990	-	-
BHmax, Maximum Energy Product	MGOe	28	31	33
	kJ/m^3	223	243	263

Table-1: b) Thermal and specific characteristics of N30UH [7]

Thermal and Specific Characteristics	Units	C // C ⊥
Reversible Temperature Coefficients (1)	-	-
Induction, α(Br)	%/ºC	-0.12
Coercivity, α(Hcj)	%/ºC	-0.51
Coefficient of Thermal Expansion (2)	ΔL/L per ºCx10^{-6}	7
Thermal Conductivity	kcal/mhrºC	5.3
Specific Heat (3)	cal/gºC	0.11
Curie Temperature, Tc	ºC	310
Flexural Strength	MPa	2 285
Density	g/m^3	7.6
Hardness and Vickers	Hv	620
Electrical Resistivity, ρ	μΩ. cm	150 // 130 ⊥

Sintered Neodymium Iron Boron (N30UH) materials placed on the rotor part as permanent magnets have strong magnetic flux spreading feature. In this project, the material named N30UH is used as a permanent magnet inside the rotor. This type of magnet was developed and released by Arnold Magnetic Technologies Corporation. In the Table-1 on below, the properties of the material named Sintered Neodymium Iron Boron(N30UH) used in the analysis are available and also B-H curve of N30UH shown in Figure-3.

The numbered parameters are respectively; (1) Coefficients measured between 20ºC and 180 ºC, (2) Between 20ºC and 200ºC, values are typical and can vary and (3) Between 20ºC and 140 ºC were observed by Arnold Magnetic Technologies Corporation.

5. Design of IPMSM using ANSYS motor-CAD

The first step in the ANSYS Motor-CAD interface is model selection. In the first part of this analysis, the E-Magnetic section was chosen because the design and input parameters of the motor will be entered into the interface and electromagnetic analysis will be made. The E-Magnetic section in ANSYS Motor-CAD allows and provide 2D finite element analysis (FEA) to obtain the operation conditions and performance of the machine. This section also has an automatic link to the thermal model in ANSYS Motor-CAD for subsequent thermal analysis. In the E-Magnetic section, the stator and rotor geometric parameters are entered. The motor length was entered as 260 mm in this section. Then the winding design is made for the stator and then the material data are entered. The data are respectively; the rotor and stator's steel type, the rotor's magnet material and the stator's winding material. Finally, the necessary parameters are entered in the calculation section and the analytical analysis is completed.

5.1. Stator

Stator is the stationary part of the PMSM. Stator of the IPMSM is distributed winding, while designing the core of the stator, the material called 30DH was used in the application. The B-H curve of this material is shown in Figure-4. The stacking factor is the ratio of the effective cross-sectional area of the stator core to the physical cross-sectional area of the stator core. The stator parameters of IPMSM shown in Table-2.

5.2. Winding

In this three phase IPMSM, there are 8 coils per phase because of slot number. This can be observed in Figure-6. There are three possible connections but we must consider to DC bus voltage and this value of parameter is shown in Table-5. Take this into account, most proper winding type is" The stator windings are connected every 2 coils in series and then the 4 branches connected in parallel to each phase". Stator winding number of turns per phase can be calculated from the no load root mean square (RMS) voltage induced in per phase of the stator winding(E) by the magnetic flux(Φf) of the rotor is calculated by equation in (2).

Table-2: Stator parameters

Stator	Values	Units
Outer Diameter	198	mm
Inner Diameter	132	mm
Stator Lenght	160	mm
Stacking Factor	0.97	-
Number of Slots	48	-
Skew Width	0	mm
Tooth Width	4.15	mm
Slot Depth	21.2	mm
Slot Corner Radius	2	mm
Tooth Tip Depth	1.2	mm
Slot Opening	2.814	mm
Tooth Tip Angle	27	-
Sleeve Thickness	0	mm
Steel Stype	30DH	-

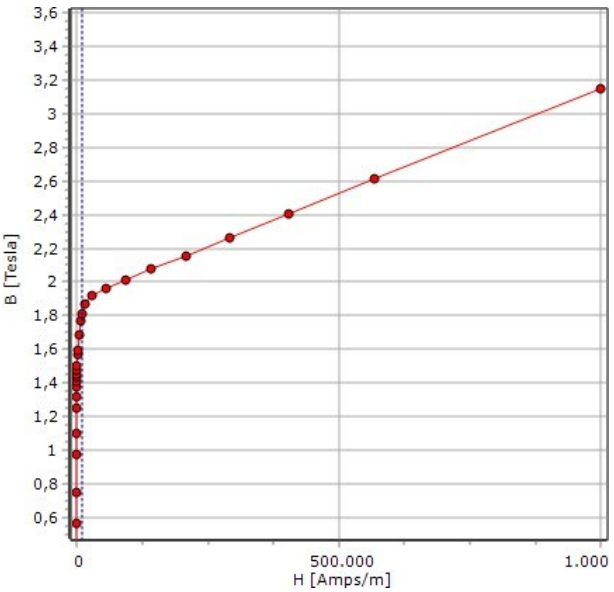

Figure-4:B-H curve of 30DH material

$$E = \pi.\sqrt{2}\,.f.N1.kw1.\Phi f \quad (2)$$

where N1 is the number of the stator turns per phase, f is electrical frequency, kw1 is winding factor of the stator and Φf is magnetic flux of rotor [8].

Magnetic flux of rotor(Φf) can be calculated permanent magnet of the rotor for IPSM by the magnetic flux density of rotor is

$$B = \Phi f.A \quad (3)$$

where Φf is magnetic flux density of permanent magnet in rotor and A is area of permanent magnet of rotor. The conductors per slot value is equal to the number of turns in each slot multiplied by the number of strands. The winding parameters of IPMSM shown in Table-3.

Table-3: Winding parameters

Winding Parameters	Values	Units
Winding Layer	1	-
Winding Type	Lap	-
Conductors Per Slot	120	-
Parallel Paths	2	-
Coil Style	Stranded	-
Throw	5	-
Wire Gauge	0.885-0.800	mm
Number of Strands	20	-
Conductor Separation	0.02	mm
Phase Numbers	3	-
Copper Depth	100	%

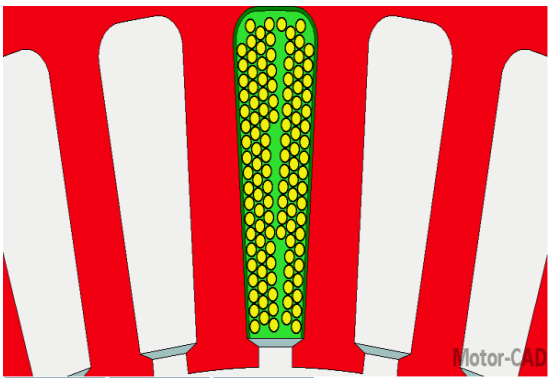

Figure-5: Winding definition for a Slot

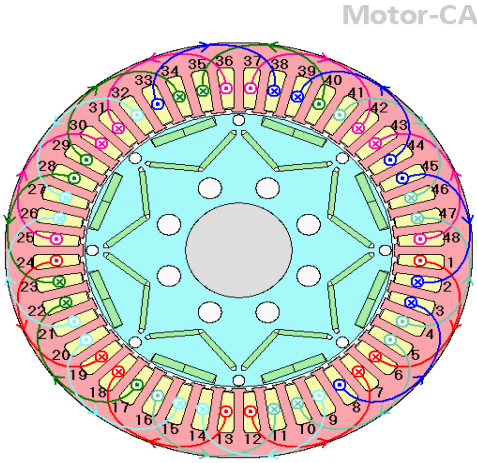

Figure-6: Winding configuration 2D pattern

5.3. Rotor

In the rotor design, V type magnets design is used as permanent magnet type. The magnetic circuit of the rotor is made up of eight sets of three permanent magnets placed in an inverted triangle configuration. This arrangement allows the magnetic torque as well as reluctance torque to be used, resulting in high power and high torque density. In order to provide adequate anti centrifugal strength while reducing magnetic flux leakage, the bridge design at both ends of the magnets where stress focuses during high-speed operation, has been improved. The poles are located in the IPMSM rotor part and materials with strong magnetic flux spreading feature should be selected. In the project, the material named N30UH is used as a permanent magnet inside the rotor. The B-H curve of material is shown in Figure-3. The number magnet of layers was entered as second laminated form of rotor and stator cores reduce to Eddy currents in rotor and stator. Therefore, stacking factor must consider to in rotor and stator. Ducts on rotor laminations hold permanent magnets, reduce to temperature of rotor and also obstruct to the d-axis flux (polar axis) due to stator current. That's why, they are also called flux barriers in literature [4]. The rotor parameters of IPMSM shown in Table-4.

Table-4: The rotor parameters of IPMSM

Rotor Parameters	Values	Units
Outer Diameter	131	mm
Inner Diameter	45	mm
Magnet Length	150	mm
Pole Number	8	-
Stacking Factor	97	%
Magnet Layers	2	-
Steel Type	30DH	-
L1-L2 Magnet Thicknesses	2.6-3.862	mm
L1-L2 Magnet V Widths	21.33-20.85	mm
L1-L2 Magnet Shifts	0-0	mm
L1-L2 Magnet Bar Widths	20.88-13.9	mm
L1-L2 Bridge Thicknesses	7.65-0.6	mm
L1-L2 Web Thicknesses	2.5-21	mm
L1-L2 Web Lengths	0-0	mm
L1-L2 Pole V Angles	124-180	o
L1-L2 Pole Arcs	159-150	o
L1-L2 Magnet Posts	0-0	mm
L1-L2 Magnet Separations	0-0	mm
L1-L2 Outer Extensions	2-1	mm
L1-L2 Inner Extensions	2-1	mm

6. Analysis of Various Parameters of IPMSM

In the analysis section of the project, IPMSM

must be consider on under no load, rated load, overload and flux weakening conditions. So as to verify, whether the motor structure meets the requirements of electric vehicle driving conditions and then optimization is performed to improve analysis results or to optimize parameters. In the process of analysis, necessary analyzes were carried out in the calculation tab under the E-Magnetic section of ANSYS Motor-CAD analysis to IPMSM. The Calculation tab provides to select the operating conditions and simulations to run are. There are many different electromagnetic FEA calculations which can be performed in ANSYS Motor-CAD. The phasor diagram is shown in Figure-7.

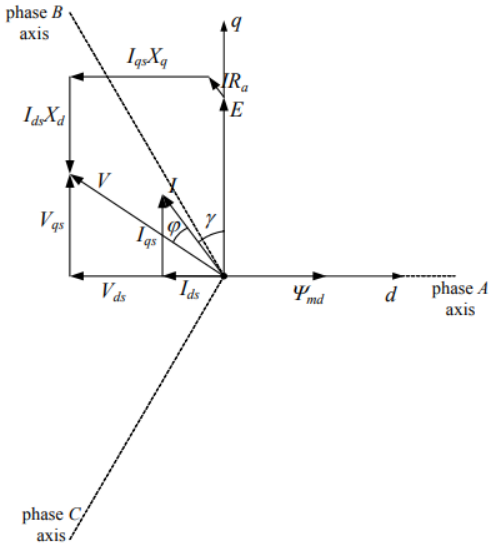

Figure-7: The phasor diagram of IPMSM [9]

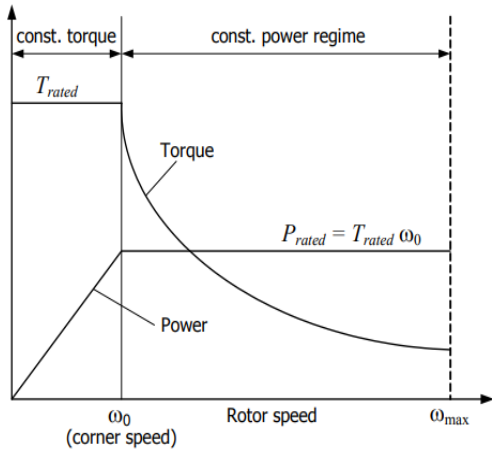

Figure-8: The operation characteristic plot of IPMSM [9]

The relation between angular speed, power and torque of IPMSM is given by equation (1).

$$P = \omega . T \quad (1)$$

Where P is average electrical output power, ω is electrical frequency in radians per second or angular speed and T is electromagnetic torque.

Output torque of the IPMSM is expressed equation (2) [4].

$$T = \frac{m}{2} . p. (\Psi_d . Iq - \Psi_q . I_d) \quad (2)$$

$$\Psi_d = \Psi_{PM} + L_d . I_d \quad (3)$$

$$\Psi_q = L_q . I_q \quad (4)$$

Ψ_{PM} is the flux linked by the d-axis winding due to the magnetizing current only, m is number of phases, p is number of pole pairs and Lq, Ld and Id, Iq are inductances and currents of d (director polar) and q (quadrature or interpolar) axises respectively [4].

The electromagnetic torque equation can be expressed another equation in terms of inductances is

$$T = m. p. (\lambda_m . I_q + \left(I_d . I_q . \left(L_d - L_q\right)\right)) \quad (5)$$

λ_m is armature interlinkage flux from permanent magnets expressed in terms of d axis and q axis.

The torque ripple of IPMSM can be calculated is given by

$$T_{ripple} = \frac{T_{max} - T_{min}}{T_{avg}} \quad (5.1.)$$

T_{max} is maximum electromagnetic torque, T_{min} is minumum electromagnetic torque and T_{avg} is average electromagnetic torque.

The reluctance torque or permanent magnet torque can be calculated by

$$T = T_{PM} + T_R \quad (6)$$

Where T is electromagnetic torque, T_{PM} is permanent magnet torque and T_R is reluctance torque.

The reluctance torque of IPMSM can be calculated is given by

$$T_R = m. \frac{p}{2} . (I_d . I_q . \left(L_d - L_q\right)) \quad (7)$$

The output power of IPMSM can be calculated by

$$P = \omega . T \quad (8)$$

The terminal voltage equations of the IPMSM in steady state are expressed in equations (9), (10) and (11) [4].

$$V_q = R. I_q + \omega . \Psi_d \quad (9)$$

$$V_d = R. I_d - \omega . \Psi_q \quad (10)$$

If we neglect phase resistance (R) the magnitude of the stator voltage is given by

$$V = \sqrt{\omega^2.(V_d + V_q)^2} \quad (11)$$

The relation between armature and current of axises is given by

$$I_a = \sqrt{{I_d}^2 + {I_q}^2} \quad (12)$$

where I_a is armature current, I_d and I_q are currents of d (direct axis or polar axis) and q (quadrature axis or interpolar axis) [4].

The maximum torque per amp operation (MTPA) in this case will occur when the current phasor is shifted by an angle γ relative to the q axis but in SMPMSM the maximum torque per amp operation occurs at γ = 0 [9].

The first region of IPMSM is constant torque region. In this region, the torque is rated torque till corner speed of machine. The corner speed is rated or nominal speed of machine. The second region of IPMSM is constant power region called flux weakening region. In this region, the power is rated power till maximum speed of machine. This must be decreased to magnetic flux of armature same as armature current (Ia) because current and magnetic flux are proportional with each other in equation (7).

Over the corner(base) speed, it is possible to maintain constant power but it is not possible to develop rated torque without exceeding the voltage constraint imposed by the power supply. Moreover, the ability to maintain constant power is not universally attainable for all IPMSM designs. The maximum constant power output in the field weakening regime over corner speed will only be provided by designs that satisfy the optimal flux weakening criterion in equation (13) [9]. This condition is given by

$$\Psi_{md} = L_d.I_a \quad (13)$$

where L_d represents to d axis inductance and I_a represents to armature current in equation (13).

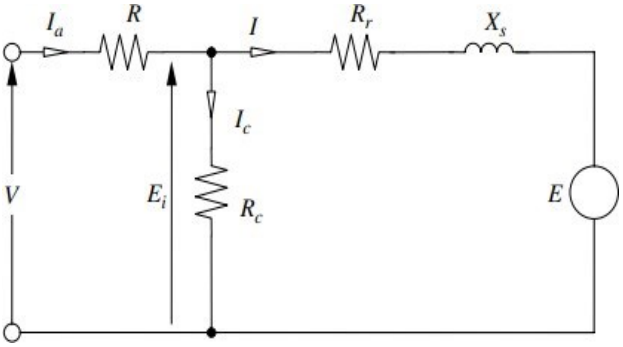

Figure-9: Equivalent Circuit per Phase of IPMSM [10]

The equivalent circuit per phase of IPMSM was given in Figure-9.

where R: winding resistance, Rc: iron loss resistance, E: permanent magnet induced EMF, Xs is total reactance, Xd: d-axis reactance, Xq: q-axis reactance.

6.1. Analysis results

The rated values of parameters assigned in IPMSM are given in the Table-5.

The maximum output power (mechanical power) of the designed motor is 80 kW, the maximum torque is 280 Nm and the top motor speed is 10000 rpm [11]. The maximum rated speed (base speed) at which this maximum torque is obtained is 2750 rpm. In order to exceed this speed, the maximum torque must be reduced. In order to reduce the maximum torque, the flux must also be weakened and the armature current (Ia) must be reduced because torque, magnetic flux and current are proportional to each other. This operation region as known as "Flux Weakening Region" of IPMSM. The efficiency and phase advance map of IPMSM in Figure-10 and Figure-11 under the 80 kW maximum power, DC bus voltage is 375 V and peak current is 480 A.

Table-5: Simulation parameters of IPMSM

Parameters	Values	Units
Rated Speed	3000	rpm
Top Speed	10000	rpm
Peak Current	480	A
DC Bus Voltage	375	V
Armature Winding Temperature	65	°C
Permanent Magnet Temperature	65	°C
Shaft Temperature	20	°C

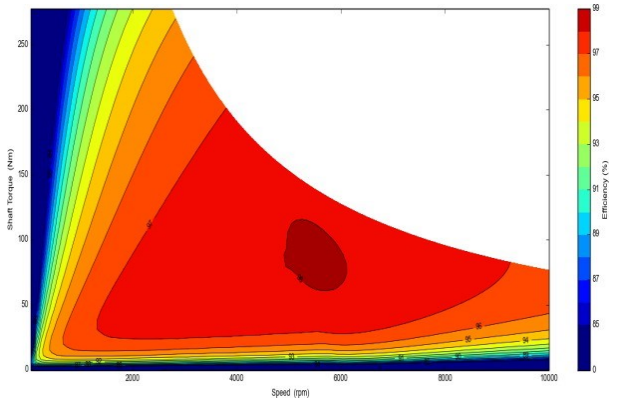

Figure-10: Efficiency map of IPMSM

In order to simulate the operating point at base speed, first the magnitude of the armature current vector I and its position relative to the q axis angle (γ) must be determined. The most

appropriate phase advance value is observed for the maximum electromagnetic torque value that can be obtained under peak current. It should be convenient to use the motor under variable speeds in the electric vehicle system, so the motor driver is used. The motor driver changes the frequency to obtain variable speed values while torque is maximum, but it can do this up to the base speed value, the torque of the motor after this value must be reduced. How this is done has been described in the previous lines.

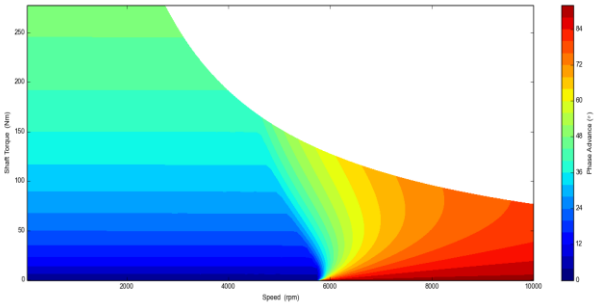

Figure-11: Phase advance(γ) map

As a result, the torque is constant until the base speed (2750 rpm). Its value is 279 Nm with variable power. The torque at top speed (10000 rpm) is 76.40 Nm. The maximum output power is 80 kW. The efficiency of the IPMSM was observed as 94.69% when operated at base speed (2750 rpm) and maximum torque of the IPMSM was observed as 277.5 Nm. Over 97% efficiency was observed when the motor was run between 5000 rpm and 9000 rpm and the torque is less compared to under the base speed, this was expected. The motor has been driven with the simulation parameters in Table-5 and the FEA results are shown below.

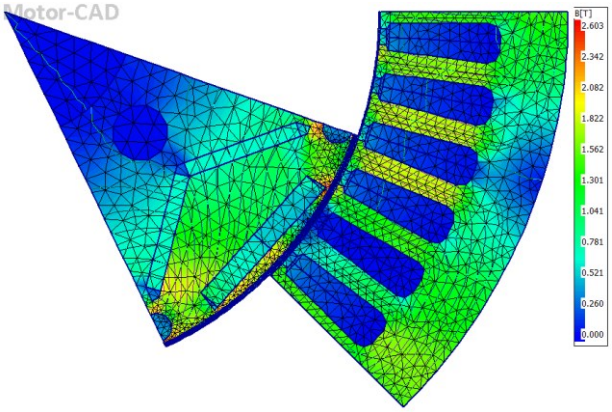

Figure-12: Magnetic flux density distribution of IPMSM on load at the simulation parameters

As it can be seen from Figure-14 and Figure-15, there are no eddy and hysteresis losses. The reason for this comes from why eddy and hysteresis losses occur.

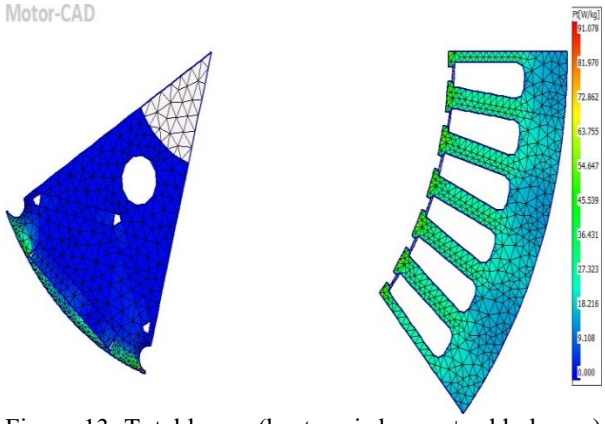

Figure-13: Total losses (hysteresis losses + eddy losses) distribution of IPMSM on load at the simulation parameters

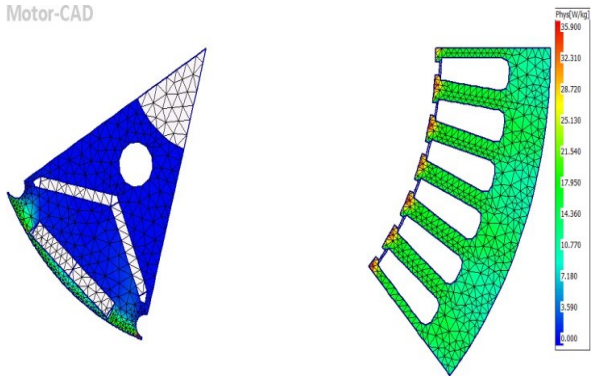

Figure-14: Hysteresis losses distribution of IPMSM on load at the simulation parameters

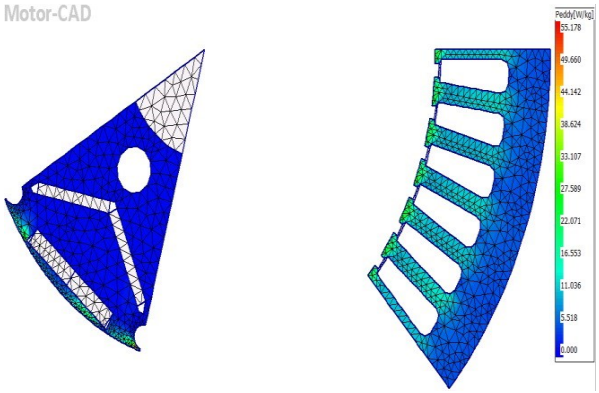

Figure-15: Eddy losses distribution of IPMSM on load at the simulation parameters

The back EMF and its waveform are important parameter for optimum motor design. The waveform of back EMF must be close to waveforms of phase-to-phase supply voltages. The three waveforms of back EMFs were shown in Figure-16. The rotation of rotor causes to induce back EMF on the stator windings. The back EMF values are lower than phase to phase supply voltages. That's why, this operation is motor operation clearly and operates as under excited. The back EMF waveforms are close to sinusoidal waveform and waveform of phase-to-

phase supply voltages. This can be seen when looking at Figure-16.

The magnetic flux density in airgap is plotted to observe effects of magnetic flux of permanent magnets during operation at 0 rpm from 0° to 360°. As a result, its waveform is smooth, this was shown in Figure-18.

Another important parameter is cogging torque, the cogging torque is largely due to the attractive force between the permanent magnets mounted on the rotor and the steel teeth of the stator laminations and when you turn the shaft of the IPMSM, you can physically feel this cogging as an intermittent jerk motion. Coreless motors do not have this quality. The rotor can rotate freely when not energized because there is no interaction between the permanent magnets and the non-magnetic stator coils. On the other hand, cogging torque is the torque produced in the no load condition and the peak-to-peak value is used to evaluate it. It is 20 Nm. Due to cogging torque is a main component of torque ripple, it is usually desired to minimize in design process. During all the speed range, the amplitude or waveform of the cogging torque does not change but the rotation speed varies depending on the frequency, the cogging torque waveform was shown in Figure-19.

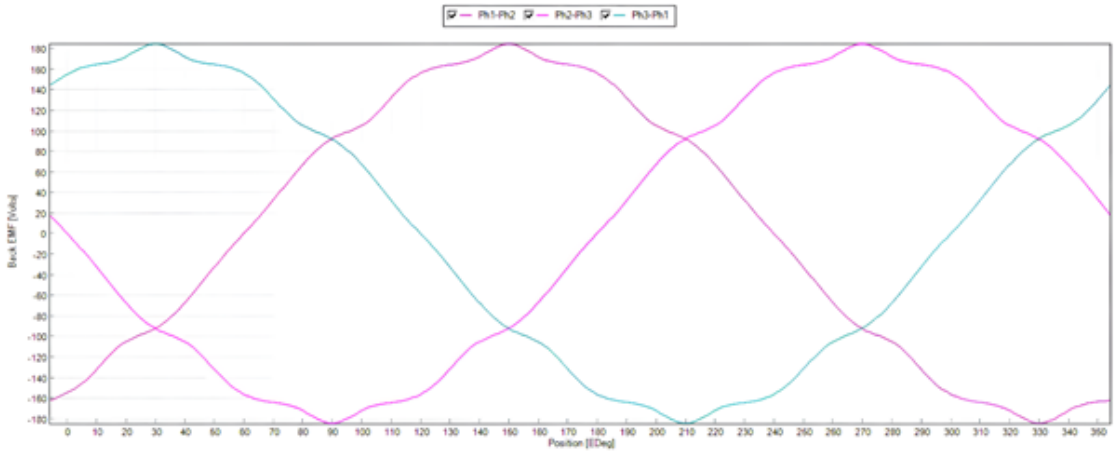

Figure-16: Back EMF waveforms of phases on open circuit operation

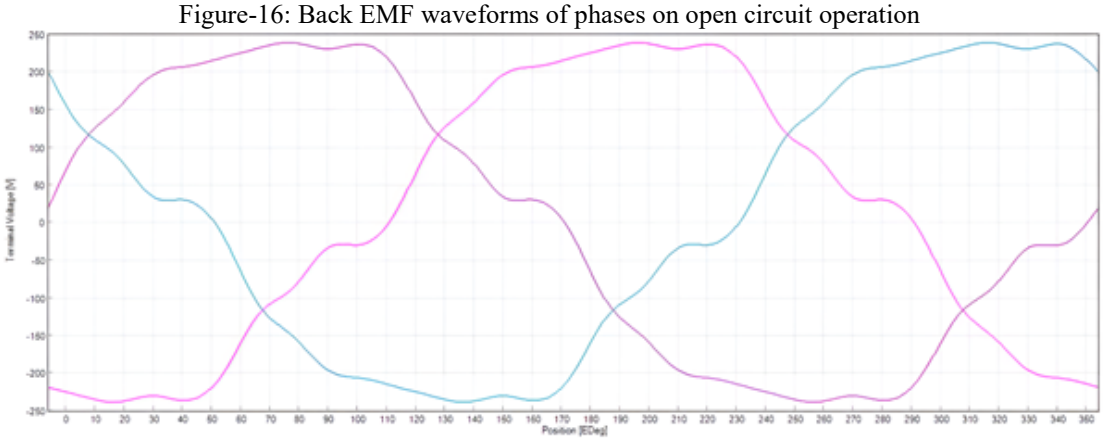

Figure-17: Terminal voltages waveforms under load

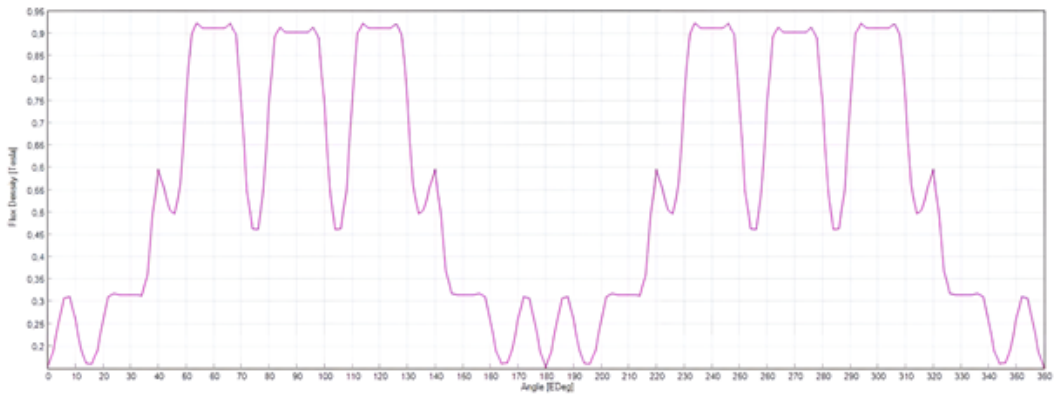

Figure-18: Magnetic flux density in airgap at locked rotor test

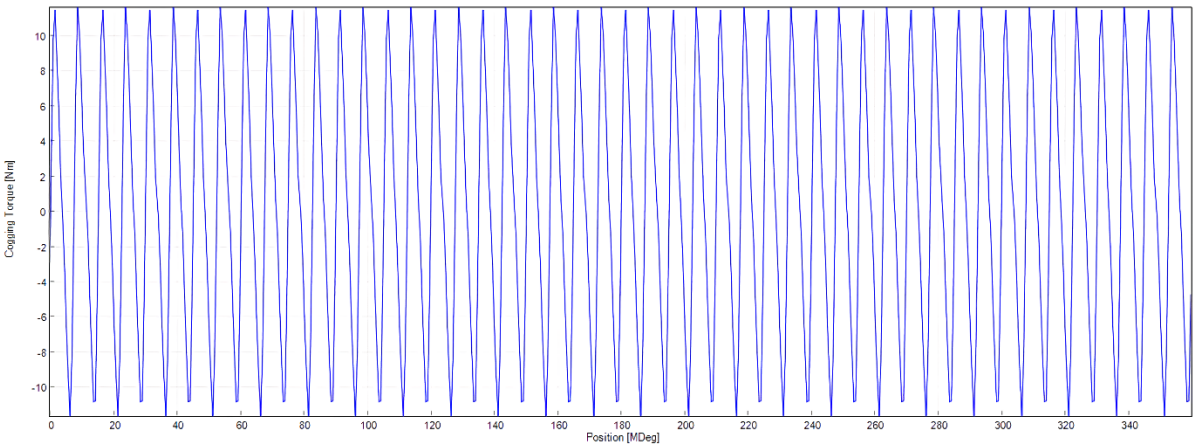

Figure-19: Cogging torque waveform

7. Optimization of IPMSM

7.1. Geometry optimization in rotor of IPMSM

The geometry optimization of the motor enables by using a composite cost function to achieve a good compromise between the two important parameters of performance and efficiency [12]. Sensitivity analysis is performed in order to choose critical design parameters, to maximize efficiency, driving torque and to minimize size. In this section, the sensitivity analysis of rotor geometrical parameters for IPMSM is investigated and considered. The geometrical parameters of the rotor can be determined with a considerable measure of freedom. The IPMSM's V shaped permanent magnet rotor aids in concentrating the magnetic flux to the rotor surface because of the flux-focusing effects and produce reluctance torque because of magnets shape. The angle between the two permanent magnets under each pole is a significant geometrical feature since it controls the magnetic circuit structure in both d axis and q axis. Although a narrow magnetic barrier might reduce magnetic flux leakage and it also has a lower mechanical strength, particularly in the high-speed range. Therefore, six rotor geometrical parameters, as shown in Figure-20 are selected to be investigated in this paper, namely the L1 and L2 magnets pole V angles (θ), the width of magnetic barrier (Wb), the thickness (Hm) and length of permanent magnets (Lm). It should be considered and noted that when one of them changes, the others are fixed [13]. The channel opened for the permanent magnets in the rotor is fixed, the Wb value changes with the change of Lm. Here, the length of the magnet inside the channel changes. Therefore, the channel opened for L1 is 21.9 mm, while the channel opened for L2 is 14.7 mm. The channel lengths for permanent magnets in rotor are determined automatically according to the number of poles and rotor diameter for a proper geometry in ANSYS Motor-CAD.

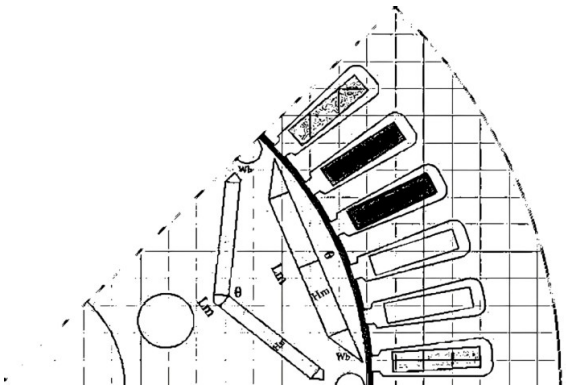

Figure-20: Geometrical parameters of IPMSM

7.1.1. Airgap of IPMSM

Airgap distance is an important parameter to efficiency of IPMSM. Airgap distance directly affects the efficiency of the motor. The reluctance value decreases when the airgap distance is reduced. The same output power is obtained with less input power with the decrease of the reluctance value. This causes to increase efficiency of motor. The torque changes with the air gap change. The reason for this is the change of the reluctance torque with the reluctance of the d axis and q axis. The reluctance torque has a very high effect on the motor torque. In this section, since the reluctance values of the d axis and q axis change with the air gap, a high output torque is obtained at a low airgap distance but the cogging torque value also increases, which increase to the torque ripple. This is not a good thing either for the motor. This was shown in

Figure-20. On the other hand, iron losses are an important parameter in changing the total losses of the motor. Iron losses depend on air gap distance. Iron losses decrease when air gap distance is increased. The effect of the change of the airgap parameter on the motor parameters has been observed and the values are shown in Table-6. The best air gap distance should be 0.85 mm after considered all the variables.

7.1.2. L1 and L2 magnet pole V angles of IPMSM

The performance characteristics of the IPMSM with different magnet pole angles at the base speed are listed in Table-7 and Table-8. In the table, L1 represents the magnet close to the shaft (inner magnet), while L2 represents the outer magnet. As a result of the examinations and evaluations, they were concluded that the L1 Pole V Angle value should be 140° and the L2 Pole V Angle value should be 170°.

7.1.3. L1 and L2 magnet thicknesses of IPMSM

The performance characteristics of the IPMSM with different magnet thicknesses at the base speed are listed in Table 9 and Table 10.

As a result of the examinations and evaluations, they were concluded that the value of L1 magnet thickness should not be changed, it should remain 2.6 mm and the L2 magnet thickness value should be 3.5 mm.

Table-6: Changing of various parameters with airgap length

Parameters	Units	Values							
Airgap	mm	0.75	0.8	0.85	0.9	0.95	1	1.05	1.1
Shaft Speed	rpm	2750	2750	2750	2750	2750	2750	2750	2750
Input Power	Watts	86632	86254	85797	85237	84775	84257	83757	83206
Total Losses (on load)	Watts	4522	4516.2	4511.5	4511	4506.4	4502	4497	4493
Output Power	Watts	82110	81737	81285	80725	80268	79755	79260	78712
System Efficiency	%	94.78	94.764	94.742	94.708	94.684	94.657	94.631	94.6
Shaft Torque	Nm	285.13	283.83	282.26	280.32	278.73	276.95	275.23	273.33
Cogging Torque Ripple (Vw)	Nm	21.977	21.304	20.365	21.783	20.768	19.816	18.734	17.866
Torque Ripple (MsVw)	Nm	13.671	13.103	12.326	13.146	11.692	11.364	12.354	13.449
Airgap Flux Density (peak)	T	1.399	1.379	1.357	1.362	1.342	1.326	1.31	1.299
D Axis Inductance	mH	0.1492	0.1496	0.1503	0.1507	0.1514	0.1521	0.1527	0.1534
Q Axis Inductance	mH	0.3582	0.3571	0.3558	0.3548	0.3535	0.3521	0.3507	0.3491
Magnet Loss (on load)	Watts	2.898	2.518	2.261	2.189	1.953	1.819	1.603	1.495
Stator iron Loss [total] (on load)	Watts	303.1	299.9	296.6	296	292.8	289.7	286.5	283.4
Rotor iron Loss [total] (on load)	Watts	29.91	27.77	26.58	26.7	25.59	24.35	23.01	22.41
Armature DC Copper Loss (on load)	Watts	4176	4176	4176	4176	4176	4176	4176	4176
Total Losses (on load)	Watts	4522	4516	4512	4511	4506	4502	4497	4493

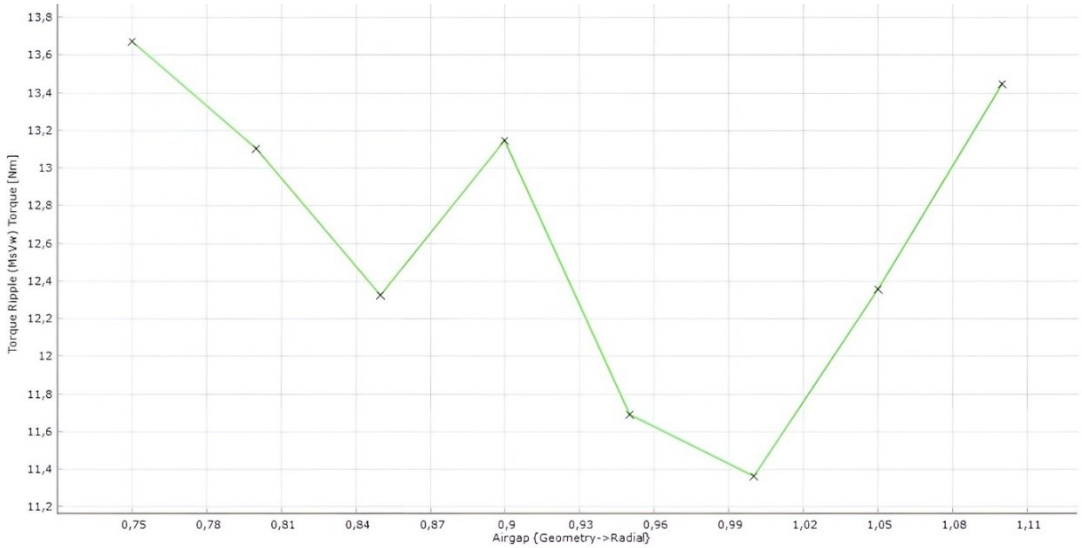

Figure-21: Torque ripple plot

The changing reason of L2 magnet thickness is cost of magnets, produce magnets with a thickness of 3.862 mm magnets must be very difficult in real life and torque ripple. The performance characteristics were shown in Table-10.

7.1.4. L1 and L2 magnet bar widths (WB) of IPMSM

The performance characteristics of the IPMSM with different magnet bar widths of L1 and L2 at the base speed are listed in Table-11 and Table-12.

As a result of the examinations and evaluations, they were concluded that the value of magnet bar width of L1 should be changed with 21 mm and the L2 magnet thickness value should be 13,8 mm. The reason of changes can realize from results of various parameters.

Table-7: Changing of various parameters with different L2 pole V angle

Parameters	Units	Values				
L2 Pole V Angle(θ)	°	160	165	170	175	180
Shaft Speed	rpm	2750	2750	2750	2750	2750
Input Power	Watts	85501	85772	85805	85809	85713
Total Losses (on load)	Watts	4518.4	4512.2	4507.7	4501.9	4496.6
Output Power	Watts	80983	81260	81297	81307	81217
System Efficiency	%	94.715	94.739	94.747	94.754	94.754
Shaft Torque	Nm	281.21	282.17	282.3	282.34	282.02
Cogging Torque Ripple (Vw)	Nm	18.713	19.632	19.777	19.911	20.365
Torque Ripple (MsVw)	Nm	13.292	12.361	10.86	12.642	18.271

Table-8: Changing of various parameters with different L1 pole V angle

Parameters	Units	Values							
L1 Pole V Angle(θ)	°	112	116	120	124	128	132	136	140
Shaft Speed	rpm	2750	2750	2750	2750	2750	2750	2750	2750
Input Power	Watts	85186	85465	85593	85805	86025	86218	86271	86414
Total Losses (on load)	Watts	4507.7	4507.4	4507.6	4507.7	4508.1	4508.5	4508.5	4508.2
Output Power	Watts	80678	80957	81085	81297	81517	81710	81762	81906
System Efficiency	%	94.708	94.726	94.734	94.747	94.76	94.771	94.774	94.783
Shaft Torque	Nm	280.15	281.12	281.57	282.3	283.06	283.73	283.92	284.41
Cogging Torque Ripple (Vw)	Nm	19.738	19.72	19.739	19.777	19.834	19.856	19.826	19.888
Torque Ripple (MsVw)	Nm	9.6685	10.313	10.357	10.86	10.449	11.171	11.214	10.799

Table-9: Changing of various parameters with different L1 magnet thickness

Parameters	Units	Values					
L1 Magnet Thickness (Hm)	mm	2	2.2	2.4	2.6	2.8	3
Shaft Speed	rpm	2750	2750	2750	2750	2750	2750
Input Power	Watts	84953	85489	85974	86809	87166	87166
Total Losses (on load)	Watts	4509.6	4508.4	4508.4	4508	4507.8	4507.8
Output Power	Watts	80444	80981	81466	82301	82658	82658
System Efficiency	%	94.692	94.726	94.756	94.807	94.828	94.828
Shaft Torque	Nm	279.34	281.2	282.89	284.41	285.79	287.03
Cogging Torque Ripple (Vw)	Nm	19.413	19.592	19.737	19.888	20.001	20.105
Torque Ripple (MsVw)	Nm	9.377	9.428	10.632	10.799	11.397	11.881

Table-10: Changing of various parameters with different L2 magnet thickness

Parameters	Units	Values												
L2 Magnet Thickness (Hm)	mm	2.8	2.9	3	3.1	3.2	3.3	3.4	3.5	3.6	3.7	3.8	3.862	3.9
Shaft Speed	rpm	2750	2750	2750	2750	2750	2750	2750	2750	2750	2750	2750	2750	2750
Input Power	Watts	83051	83460	83865	84246	84546	84943	85219	85443	85785	86024	86292	86414	86525
Total Losses (on load)	Watts	4512.6	4511.7	4511.2	4510.8	4510.5	4510.2	4509.9	4509	4508.7	4508.3	4508.1	4508.2	4508.7
Output Power	Watts	78539	78949	79354	79735	80036	80433	80709	80934	81277	81516	81784	81906	82016
System Efficiency	%	94.566	94.594	94.621	94.646	94.665	94.69	94.708	94.723	94.744	94.759	94.776	94.783	94.789
Shaft Torque	Nm	272.72	274.15	275.55	276.88	277.92	279.3	280.26	281.04	282.23	283.06	283.99	284.41	284.8
Cogging Torque Ripple (Vw)	Nm	17.715	18.001	18.283	18.413	18.639	18.905	19.008	18.974	19.535	19.754	19.973	19.888	20.206
Torque Ripple (MsVw)	Nm	7.2449	7.1385	7.6938	8.6956	9.0053	9.3386	9.3592	9.6972	10.137	10.664	10.849	10.799	11.315

Table-11: Changing of various parameters with different magnet bar width of L1 magnet bar widths maximum value of L1 is 21.9 mm

Parameters	Units	Values											
L1 Magnet Bar Width(Wb)	mm	19	19.2	19.4	19.6	19.8	20	20.2	20.4	20.6	20.8		20.88
Shaft Speed	rpm	2750	2750	2750	2750	2750	2750	2750	2750	2750	2750		2750
Input Power	Watts	83361	83575	83800	84042	84273	84466	84725	84914	85076	85369		85443
Total Losses (on load)	Watts	4509	4508.6	4508.5	4508.3	4508.7	4508.8	4508.9	4509	4508.2	4509.1		4509
Output Power	Watts	78852	79067	79291	79534	79764	79957	80216	80405	80568	80860		80934
System Efficiency	%	94.591	94.605	94.62	94.636	94.65	94.662	94.678	94.69	94.701	94.718		94.723
Shaft Torque	Nm	273.81	274.56	275.34	276.18	276.98	277.65	278.55	279.2	279.77	280.78		281.04
Cogging Torque Ripple (Vw)	Nm	17.556	17.702	17.845	17.987	18.157	18.314	18.45	18.606	18.715	18.943		18.974
Torque Ripple (MsVw)	Nm	7.939	8.1653	8.6617	8.565	8.8782	9.1565	9.0234	8.9764	10.064	9.4382		9.6972

Table-12: Changing of various parameters with different magnet bar width of L2 magnet bar width maximum value of L2 is 14.7 mm

Parameters	Units	Values											
L2 Magnet Bar Width(Wb)	mm	13.5	13.6	13.7	13.8	13.9	14	14.1	14.2	14.3	14.4	14.5	14.6
Shaft Speed	rpm	2750	2750	2750	2750	2750	2750	2750	2750	2750	2750	2750	2750
Input Power	Watts	85146	85267	85424	85531	85504	85624	85747	85844	85997	86042	86148	86233
Total Losses (on load)	Watts	4511	4510.5	4510.6	4509.7	4509.1	4508.1	4508.5	4507.1	4506.9	4506.3	4505.6	4504.9
Output Power	Watts	80635	80757	80914	81021	80995	81116	81238	81337	81490	81536	81643	81728
System Efficiency	%	94.702	94.71	94.72	94.727	94.726	94.735	94.742	94.75	94.759	94.763	94.77	94.776
Shaft Torque	Nm	280	280.43	280.97	281.34	281.25	281.67	282.1	282.44	282.97	283.13	283.5	283.8
Cogging Torque Ripple (Vw)	Nm	15.445	16.387	17.095	18.205	19.022	20.227	21.511	22.524	22.805	24.166	23.481	23.243
Torque Ripple (MsVw)	Nm	13.096	12.328	11.126	9.0327	9.61	11.423	13.247	14.919	16.126	19.014	19.885	21.968

7.1.5. Combined sensitivity analysis results of IPMSM

Airgap and various geometry analyze were performed for IPMSM and the best values were tried to be selected by considering various parameters as a result of the obtained parameter values. As a result, the efficiency of our machine has increased noticeably, torque ripple has decreased and iron losses have also decreased. The analysis made for the parameters obtained at the end and the results obtained can be observed from the various plots below. As a result, the torque is constant until the base speed (2750 rpm). Its value is 279.98 Nm with variable power. The torque at top speed (10000 rpm) is 76.39 Nm. The maximum output power is 80.63 kW. The efficiency of the IPMSM was observed as %95.908 when operated at base speed (2750 rpm) and maximum torque of the IPMSM was observed as 279.98 Nm. Over %97 efficiency was observed when the motor was run between 5000 rpm and 9000 rpm and the torque is less compared to under the base speed, the result is expected.

The motor has been driven with the simulation parameters in Table-13, the simulation results are shown in Table-14 and FEA results are shown on below.

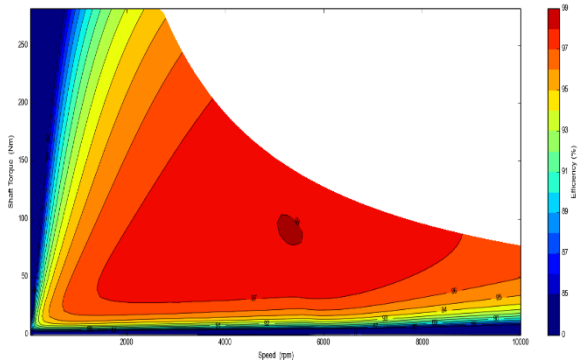

Figure-22: Efficiency map of IPMSM after optimization

Table-13: Simulation parameters of IPMSM

Parameters	Units	Values
Rated Speed	rpm	3000
Top Speed	rpm	10000
Peak Current	A	480
DC Bus Voltage	V	375
Armature Winding Temperature	°C	65
Permanent Magnet Temperature	°C	65
Shaft Temperature	°C	20

As a result, as can be seen from the plots and figures, the air gap flux density value increased. Torque fluctuation and cogging torque decreased. Therefore, the output torque increased and reached a more stable form and increased efficiency.

Table-14: Simulation results of IPMSM

Parameters	Units	Values
Shaft Speed	rpm	2750
Shaft Torque	Nm	279.98
Shaft Power	Watts	80600
Input Power	Watts	84070
Stator Copper Loss	Watts	4110
Iron Loss	Watts	317.2
Total Loss	Watts	4439
Efficiency	%	95.908

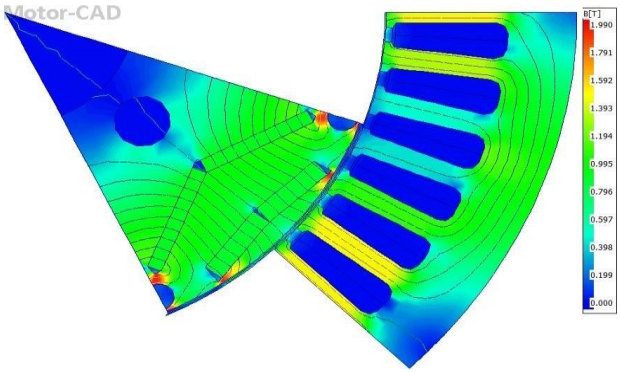

Figure-23: Magnetic flux density distribution of IPMSM on load at the simulation parameters after optimization

8. Conclusion

In the article, some analysis and improvements were made on the IPMSM, which was previously designed and produced for the LEAF model electric vehicle by the Nissan company.

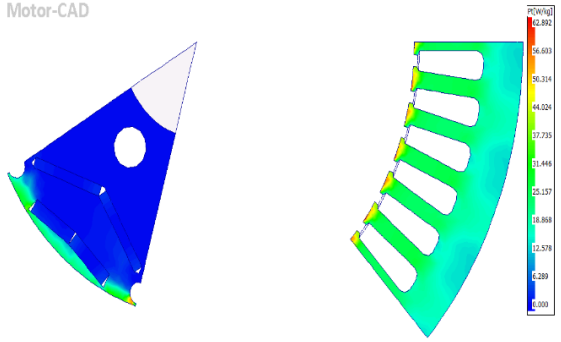

Figure-24: Total losses (hysteresis losses + eddy losses) distribution of IPMSM on load at the simulation parameters after optimization

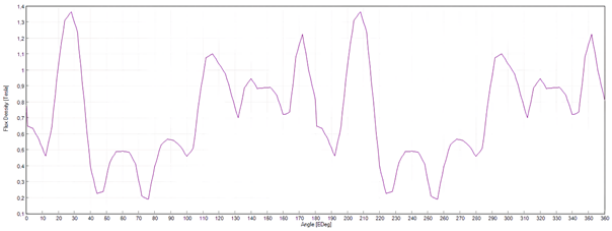

Figure-25: Magnetic flux density in airgap at locked rotor test after optimization

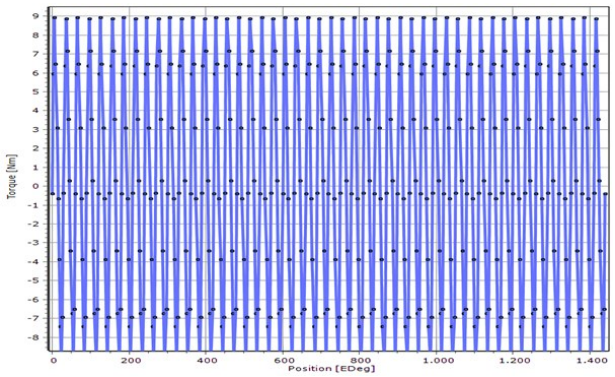

Figure-26: Cogging torque waveform after optimization

Starting from the structure of the IPMSM, working principle, structural and parametric analysis were made. Afterwards, the results were optimized and the best value obtained for each parameter was replaced with the non-good value obtained from the previous analysis before sensitivity analysis of the next parameter was performed.

The airgap distance between the rotor and the stator and the change of the permanent magnets in the rotor were emphasized and the best parameters were selected with the optimization. The results were as expected. The airgap distance was reduced from 1 mm to 0.85 mm, resulting in reduced copper losses and increased airgap magnetic flux density. The iron losses were slightly increased with this but the effect

was less on efficiency compared to copper losses. As a result, the reduction in total loss and therefore the increase in efficiency comes from the definition of efficiency. Also, the airgap distance was reduced to increase the airgap flux density and output torque increased with the airgap flux density is increased. The sensitivity analysis was performed for the optimization of permanent magnets on ANSYS Motor-CAD. The torque ripple value of the motor was reduced and with the results obtained. Since the torque ripple and cogging torque was reduced, a more stable torque value was observed at the output. The cost of permanent magnets has decreased due to advances in permanent magnets. Many more optimizations can be made within the motor. In the paper, optimization has been made on various parameters mentioned in the previous lines.

Acknowledgment

This project was not supported by any organization and institution.

CRediT authorship contribution statement

The author certifies that literature review, analysis, design, optimization, writing, revision of the manuscript processes conducted by him. Declaration of Competing Interest The author declare that they have no known competing financial interests or personal relationships that could have appeared to influence the work reported in this paper.

9. References

1. Gieras, J.F."Permanent Magnet Motor Technology: Design and Applications", Taylor&Francis, 26/08/2009.
2. Paplicki, Piotr & Piotuch, Rafał. "Improved Control System of PM Machine with Extended Field Control Capability for EV Drive", Springer, Cham, AISC,volume 317, 1-2, 2015.
3. A. Loganayaki and R. B. Kumar, "Permanent Magnet Synchronous Motor for Electric Vehicle Applications," 2019 5th International Conference on Advanced Computing & Communication Systems (ICACCS), 1064-1069, 2019.
4. Bianchi, N. "Electrical Machine Analysis Using Finite Elements", Taylor&Francis, 31/01/2017.
5. Fleisch, Daniel. "A Student's Guide to Maxwell's Equations", Cambridge University Press, 2008.
6. Shinde, Prajakta Shankar, A. G. Thosar, and Punit Lalji Ratnani. "Design of permanent magnet synchronous motor." Int. J. Sci. Eng. Res 6.1, 2015.
7. https://www.arnoldmagnetics.com/ products/neodymium-iron-boron-magnets/ , 27/ 04 2023.
8. John M. Miller," Electric Motor R&D DOE Hydrogen and Fuel Cells Program and Vehicle Technologies Program Annual Merit Review and Peer Evaluation Meeting", Oak Ridge National Laboratory, 15/05 2013.
9. Žarko, D., Ban, D. i Klarić, R. " Finite Element Approach to Calculation of Parameters of an Interior Permanent Magnet Motor", 119 International Journal of Automotive Engineering and Technologies, 105-119, Automatika, 46, 3-4, 113-122, 2005.
10. Kondo, M. " Parameter measurements for permanent magnet synchronous machines" IEEJ Trans Elec Electronic Engineering, 2, 109-117, 2007.
11. Sato, Y., Ishikawa, S., Okubo, T., Abe, M. et al., "Development of High Response Motor and Inverter System for the Nissan LEAF Electric Vehicle," SAE Technical Paper, 2011.
12. Laskaris, Knstantinos & Haniotis, A. & Kladas, A. " High performance traction motor design and construction for small passenger electric car", 19th International Conference on Electrical Machines,11614819,1-6,2010.
13. H. Chen and C. H. T. Lee, "Parametric Sensitivity Analysis and Design Optimization of an Interior Permanent Magnet Synchronous Motor", IEEE Access, 7,159918-159929, 2019.